Drifting of the solution pattern for the nonlinear Schrödinger equation

2000 J. Phys. A: Math. Gen. 33 9119

(http://iopscience.iop.org/0305-4470/33/49/307)

J. Phys. A: Math. Gen. **33** (2000) 9119–9130. Printed in the UK PII: S0305-4470(00)14550-0

Drifting of the solution pattern for the nonlinear Schrödinger equation

Yu Tan and Jian-min Mao†

Department of Mathematics, Hong Kong University of Science and Technology, Hong Kong, People's Republic of China

E-mail: mamao@ust.hk

Received 7 June 2000, in final form 17 October 2000

Abstract. When a solution of the one-dimensional nonlinear Schrödinger equation is disturbed by a harmonic function of the space variable, the solution pattern may drift in space as time evolves. The value and the direction of the drifting velocity vary with time. To understand this phenomenon, a perturbation analysis is performed. The drifting velocity given by the analysis agrees well with the direct numerical result.

1. Introduction

The nonlinear Schrödinger (NLS) equation has been used to model many physical processes, such as optical pulse propagation in fibres or in uniform plasma [1]. Intensive studies have been made on properties of the equation and its solutions, such as soliton solutions [2–4], modulation instability of solutions [5], the homoclinic structure of the equation [6], and so on.

In our numerical studies on the one-dimensional NLS equation, we have frequently observed that if a solution of the NLS equation is disturbed by a spatially harmonic perturbation (i.e., a perturbation that is a harmonic function of spatial variable only), the pattern of the solution drifts in space as time progresses‡. Therefore we ask whether pattern drifting is a general phenomenon in the NLS equation. In this paper we first numerically study what happens when the spatially homogeneous solution of the one-dimensional cubic-repulsive NLS equation is disturbed by a spatially harmonic perturbation. We observe that pattern drifting always occurs as long as perturbation is a linear combination of the harmonic functions $\sin(kx)$ and $\cos(kx)$, where k is the wavenumber and x is the space variable, and the ratio of the two combination constants is complex. Pattern drifting is in addition to the exponential growth of the coherent structure due to the modulation instability. (Modulation instability refers to the small amplitude and phase perturbation of a soliton solution of the NLS equation that tend to grow exponentially as a result of the combined effects of the nonlinearity of the equation and diffraction (in the spatial domain)/dispersion (in the time domain) of the solution to the NLS equation.) Pattern drifting is also observed when we disturb the Jacobi elliptic-function solution of the NLS equation or the spatially homogeneous solution of the perturbed NLS equation. To understand the numerical observations of the pattern drifting, we perform further

† Corresponding author.

‡ Figure 3.3.5 of [4] was used by the book's authors to show the numerical homoclinic instability. Though not mentioned in the book, pattern drifting can be seen from the figure.

0305-4470/00/499119+12$30.00

perturbation analysis and obtain a formula for the drifting velocity. The formula agrees well with the direct numerical results. The numerical and the analytical results together show that pattern drifting is a general phenomenon in the NLS equation.

This paper is organized as follows. In section 2, we present numerical observations of pattern drifting when the spatially homogeneous solution of the one-dimensional cubic-repulsive NLS equation is disturbed by a spatially harmonic perturbation. In section 3, we give the results of the perturbation analysis (the analysis itself is presented in the appendix) and use the results to understand the numerical observations of the pattern drifting. In section 4, we numerically study pattern drifting when the Jacobi elliptic-function solution of the NLS equation is perturbed. In section 5, we numerically investigate pattern drifting when the spatially homogeneous solution of the perturbed NLS equation is disturbed. Finally, the conclusions are presented in section 6.

2. Pattern drifting for the spatially homogeneous solution

We study the one-dimensional cubic-repulsive NLS equation

$$\mathrm{i}\partial_t\psi + \partial_x^2\psi + |\psi|^2\psi = 0 \qquad -L/2 \leqslant x \leqslant L/2 \qquad t \geqslant 0 \tag{1}$$

where $\psi = \psi(x, t)$ is the wavefunction and L is the system length. In this paper, we study the equation under the periodic boundary condition. The equation has the spatially homogeneous solution

$$\psi_h(x, t) = \psi_0 \,\mathrm{e}^{\mathrm{i}|\psi_0|^2 t} \tag{2}$$

where ψ_0 is a real constant. (This solution becomes the steady-state solution $\psi(x, t) = \psi_0$ under a trivial gauge transformation.) Let the spatially homogeneous solution be perturbed at $t = 0$ so that the NLS equation has the following initial conditions:

$$\psi(x, 0) = \psi_0 + \epsilon\psi_0[Y_1 \cos(kx) + Y_2 \sin(kx)] \tag{3}$$

where ϵ is a small real parameter, k is the (real) wavenumber, and Y_1 and Y_2 are complex numbers. With these initial conditions and the periodic boundary condition, we numerically solve equation (1) by an improved split method with an accuracy of the third order in time.

The results of the numerical simulation are shown in figure 1 for the parameter values $\psi_0 = 2$, $\epsilon = 0.01$ and $k = 0.9k_0$, where $k_0 = \sqrt{2}\psi_0$ is the critical value of the wavenumber for modulation instability [7]. In all plots of the figure, modulation instability is induced and therefore a coherent structure appears as expected. At the top of each plot, the initial perturbation is specified, which is a combination of the symmetric mode $\cos(kx)$ and the asymmetric mode $\sin(kx)$. In figure 1(a), the initial perturbation contains only the symmetric mode, and the spatial structure of the solution does not move in space when time evolves as expected. In figure 1(b), however, the spatial structure of the solution drifts with time. Consequently, the reflection symmetry of the solution pattern about a line of $x =$ constant breaks. (The pattern drifting shown in figure 1(b) is a short-time behaviour: the pattern drifts less and less as time progresses.) The initial perturbation contains both the symmetric and the asymmetric modes, and the ratio of the coefficients Y_1 and Y_2 is a complex number. The drifting persists no matter how we refine the spatial resolution of the numerical scheme we use. One might guess, with good reason, that the drifting (and the consequent symmetry breaking) is to be induced whenever the initial perturbation contains the asymmetric term $\sin(kx)$. But the guess is only partially correct: containing an asymmetric mode in the initial condition is not enough, though necessary, to cause pattern drifting. This can be seen from figure 1(c), where there is no pattern drifting even though the initial perturbation contains $\sin(kx)$. Furthermore, as shown

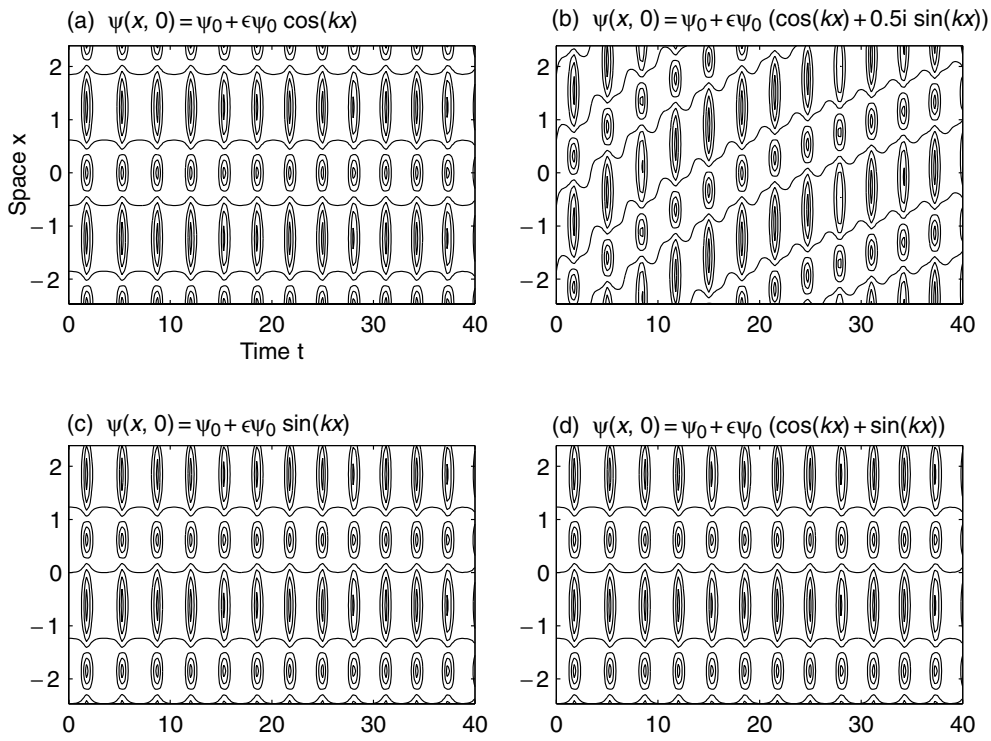

Figure 1. Contour plots of numerical solutions of the NLS equation with the initial perturbation shown at the top of each plot. The initial conditions give a spatially perturbed homogeneous solution. Pattern drifting occurs only in (*b*). Modulation instability is induced in all the plots.

in figure 1(*d*), drifting cannot be induced even when both asymmetric and symmetric modes are contained in the initial perturbation if the ratio of the coefficients, Y_1/Y_2, is a real number.

In addition to those shown in figure 1, more simulations for other choices of coefficients Y_1 and Y_2 in the initial conditions (3) have been performed. All of them show that, consistent to the observations in figure 1, pattern drifting occurs whenever the coefficients in the initial condition (3) satisfy $|Y_1| \neq 0$, $|Y_2| \neq 0$ and Y_2/Y_1 is complex.

All our numerical simulations show that pattern drifting occurs when the perturbation in equation (3) consists of both asymmetric and symmetric terms, and the coefficients of the two terms are not along the same line in the complex plane. Using the electrodynamic terminology, this kind of perturbation may be referred as 'circularly polarized', and 'linearly polarized' otherwise.

To study pattern drifting quantitatively, we trace the motion of the extremum of the initial perturbation that is closest to $x = 0$ among all extrema. The extremum moves to point A and then point B in figure 2(*a*) as time evolves, where point A is a maximum becoming a minimum later. Let $x_e(t)$ be the x-coordinate of the extremum at time t. The dotted curve in figure 2(*b*) is $x_e(t)$ from the numerical results shown in figure 2(*a*). (The continuous curve is from the perturbation analysis given in the following section.) The velocity of the pattern drifting is given by the slope of the curve for $x_e(t)$. It is clear from the figure that drifting velocity varies with time. The direction of the drifting velocity also varies with time, as can be clearly seen in figure 1(*b*).

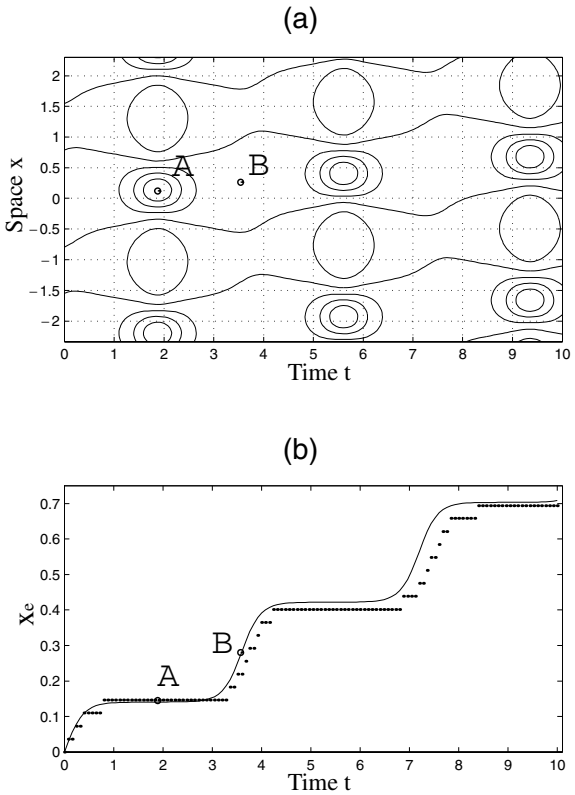

Figure 2. (*a*) A contour plot of the perturbed spatially homogeneous solution when $\psi_0 = 2$, $\epsilon = 0.01$ and $k = 0.95k_0$, similar to figure 1(*b*). (*b*) Movement of the extremum of the spatial structure of the solution closest to $x = 0$ when $t = 0$. The dotted curve is from the direct numerical simulation shown in (*a*). The solid curve is from the perturbation analysis given in section 3. The slope of the curves is the drifting velocity.

Pattern drifting should have applications in physics considering the wide use of the NLS equation in studies of a variety of physical systems. For example, the NLS equation is the governing equation for nonlinear pulses and beams of light or other electro-magnetic waves propagating in a nonlinear media such as light fibres, see Chapter 1 of [1] for details. It is well known that the NLS equation has soliton solutions of different types and a solution pattern is formed. The drifting of the solution pattern studied in this paper should therefore have applications in physics of nonlinear pulses and beams. Pattern drifting changes the location of the soliton. (Though the drifting is a short-time behaviour, the soliton, whose location moves a short time after perturbation stays in its new location for later times.) Therefore pattern drifting should play an important role in the physics of pulses and beams propagating in nonlinear media.

3. Perturbation analysis

To understand the pattern drifting phenomenon, we perform perturbation analysis. But why perturbation analysis when it is well known that the NLS equation is integrable and the solution of an integrable partial differential equation can be analytically found using the inverse

scattering method [2, 4] and the Bäcklund transformation [8–10]? The mathematical formula for the exact analytical solution is usually so complicated that it is difficult to use it to explain such a complicated phenomena such as pattern drifting and thus a perturbation method may be helpful. Our perturbation analysis follows the idea of the perturbation method introduced in [7]. The solution of the NLS equation obtained from the analysis is given in the following section, and is used in section 3.2 to derive an expression for the drifting velocity, which agrees well with the numerical results presented in the previous section.

3.1. The perturbation-analytical solution of the NLS equation

As derived in the appendix, the solution of the NLS equation with the periodic boundary condition in a neighbourhood of the spatially homogeneous solution and when the wavenumber is close to its critical value for modulation instability is given by $\psi(x,t) = \sqrt{\rho(x,t)}\exp[\mathrm{i}\theta(x,t)]$, where

$$\begin{aligned}\rho(x,t) &= N + r(t)\cos(kx-\phi(t)) + \frac{1}{4N}r^2(t)\cos 2(kx-\phi(t)) \\ &\quad + \frac{3}{64N^2}r^3(t)\cos 3(kx-\phi(t)) + \cdots \\ \theta(x,t) &= \frac{1}{4N}\int_0^t r^2(\tau)\,\mathrm{d}\tau + \frac{1}{4N^2}\partial_t[r(t)\cos(kx-\phi(t))] \\ &\quad + \frac{1}{64N^3}\partial_t[r^2(t)\cos 2(kx-\phi(t))] + \cdots .\end{aligned} \tag{4}$$

Here $N = \frac{1}{L}\int_{-L/2}^{L/2}|\psi(x,t)|^2\,\mathrm{d}x$ is the total number of quasi-particles, k is the wavenumber, and $r(t)$ and $\phi(t)$ are real functions of time, governed by Hamilton's equations with the following Hamiltonian function:

$$H(r,\phi,p_r,p_\phi) = \frac{1}{2}\left(p_r^2 + \frac{p_\phi^2}{r^2}\right) + V(r) \qquad V(r) = \tfrac{1}{8}r^4 + (\delta k)k_0^3 r^2 \tag{5}$$

where p_r and p_ϕ are momenta conjugate to r and ϕ, respectively, and $V(r)$ is the potential. The potential is ϕ-independent and therefore the angular momentum is conserved. Solution (4) is in terms of $r(t)$ and $\phi(t)$. The solution can also be written in terms of another set of functions of time, $\alpha(t)$ and $\beta(t)$, when (r,ϕ) are considered to be the polar coordinates on the $\alpha\beta$-plane. That is, $r(t) = \sqrt{[\alpha(t)]^2 + [\beta(t)]^2}$ and $\phi(t) = \tan^{-1}[\beta(t)/\alpha(t)]$.

3.2. The drifting velocity

It is clear from equation (4) that $\rho(x,t)$ reaches its maximum when $kx - \phi(t) = 0$. Therefore the location of the extremum, $x_\mathrm{e}(t)$, as defined previously, is given by

$$x_\mathrm{e}(t) = \frac{1}{k}\phi(t) \tag{6}$$

where the function $\phi(t)$ can be found numerically by solving the Hamiltonian system (5) with a given initial condition. The solid curve in figure 2(*b*) is for $x_\mathrm{e}(t)$ given by equation (6). The dotted curve in the figure, as explained previously, is from the direct numerical integration of the NLS equation. For both the curves, the initial condition is given by $\alpha(0) = 0.8$, $\beta(0) = 0$, $\dot\alpha(0) = 0$ and $\dot\beta(0) = 0$ (and then the initial conditions for $\rho(x,t)$ and $\theta(x,t)$ are given by equation (4)). Good agreement of the two curves indicates that the perturbation analysis gives a good approximation to the solution of the NLS equation.

The drifting velocity $v(t)$ is the time derivative of $x_e(t)$. Therefore,

$$v(t) = \frac{1}{k}\dot{\phi}(t) \tag{7}$$

where $\dot{\phi}(t) = [\alpha(t)\dot{\beta}(t) - \dot{\alpha}(t)\beta(t)]/r^2(t) = r^2(0)\,\dot{\phi}(0)/r^2(t)$. It is clear from equation (7) that pattern drifting is due to a rotation in the $\alpha\beta$-plane and that the drifting velocity is proportional to the angular velocity of the rotation. The rotation is a free rotation since the potential in equation (5) is ϕ-independent. One may say that pattern drifting is caused by the ignored-coordinate instability [11] because the ϕ coordinate is 'ignored' in the potential, and thus call the instability the drifting instability.

The drifting velocity can also be expressed in terms of Y_1 and Y_2, the coefficients in the initial conditions (3). To do so, we consider solution (4) for $t = \delta \approx 0$. In this case, $r(\delta)$ is small, the solution is close to the spatially homogeneous solution $\psi(x, t) = \psi_0 = \sqrt{N}$, and the quadratic and higher-order terms in $r(\delta)$ are negligible. Thus $\rho \approx N + r\cos(kx - \phi) = N + (\alpha\cos kx + \beta\sin kx)$ and $\theta \approx \frac{1}{4N^2}\partial_t[r\cos(kx - \phi)] = \frac{1}{4N^2}(\dot{\alpha}\cos kx + \dot{\beta}\sin kx)$, and

$$\begin{aligned}\psi(x,\delta) = \sqrt{N} &+ \left[\frac{1}{2\sqrt{N}}\alpha(\delta) + \frac{\mathrm{i}}{4N^{3/2}}\dot{\alpha}(\delta)\right]\cos(kx) \\ &+ \left[\frac{1}{2\sqrt{N}}\beta(\delta) + \frac{\mathrm{i}}{4N^{3/2}}\dot{\beta}(\delta)\right]\sin(kx) + \cdots.\end{aligned} \tag{8}$$

Comparing this with the initial conditions (3), we have

$$\begin{aligned}Y_1 &= \frac{1}{2\epsilon N}\alpha(0) + \frac{\mathrm{i}}{4\epsilon N^2}\dot{\alpha}(0) \\ Y_2 &= \frac{1}{2\epsilon N}\beta(0) + \frac{\mathrm{i}}{4\epsilon N^2}\dot{\beta}(0).\end{aligned} \tag{9}$$

Hence the imaginary part of $Y_1 Y_2^*$, where $*$ denotes a complex conjugate, is proportional to $\dot{\phi}(0)$, i.e., $\dot{\phi}(0) = -\frac{8\epsilon^2 N^3}{r^2(0)}|Y_1||Y_2|\sin\gamma$, where γ is the angle between the vectors representing Y_1 and Y_2 in the complex plane. equation (7) becomes

$$v(t) = -\frac{8\epsilon^2 N^3}{k\,r^2(t)}\,|Y_1||Y_2|\sin\gamma + \cdots. \tag{10}$$

Thus the drifting velocity is nonzero if and only if Y_1, Y_2 and the angle between them are all nonzero, according to the perturbation analysis. This agrees with the numerical observations shown in figure 1. Figure 1(c) is the initial conditions with $Y_1 \neq 0$, $Y_2 \neq 0$ and $\gamma \neq 0$ and therefore the pattern drifts. The pattern does not drift in figure 1(a) because $Y_2 = 0$; in figure 1(c) because $Y_1 = 0$; nor in figure 1(d) because $\gamma = 0$.

4. Pattern drifting for the elliptic-function solution

Pattern drifting can occur not only when the spatially homogeneous solution is perturbed, as discussed above, but also when the following elliptic-function solution of the NLS equation [10] is perturbed

$$\psi_e(x, t) = f(x)\mathrm{e}^{\mathrm{i}at} \qquad f(x) = \sqrt{2}b\,\mathrm{dn}(bx, c) \tag{11}$$

where a, b and c are constants (b and c are related by $b = \sqrt{a - \frac{1}{8}(1 - c)}$), and $\mathrm{dn}(\cdot,\cdot)$ is the Jacobi elliptic function. The conservation of the quasi-particle number and the periodic boundary condition requires the constants to satisfy $\frac{1}{L}\int_{-L/2}^{L/2}[f(x)]^2\,\mathrm{d}x = N$ and $\frac{4}{b}K(c) = L$, where $K(\cdot)$ is the complete elliptic integral of the first kind.

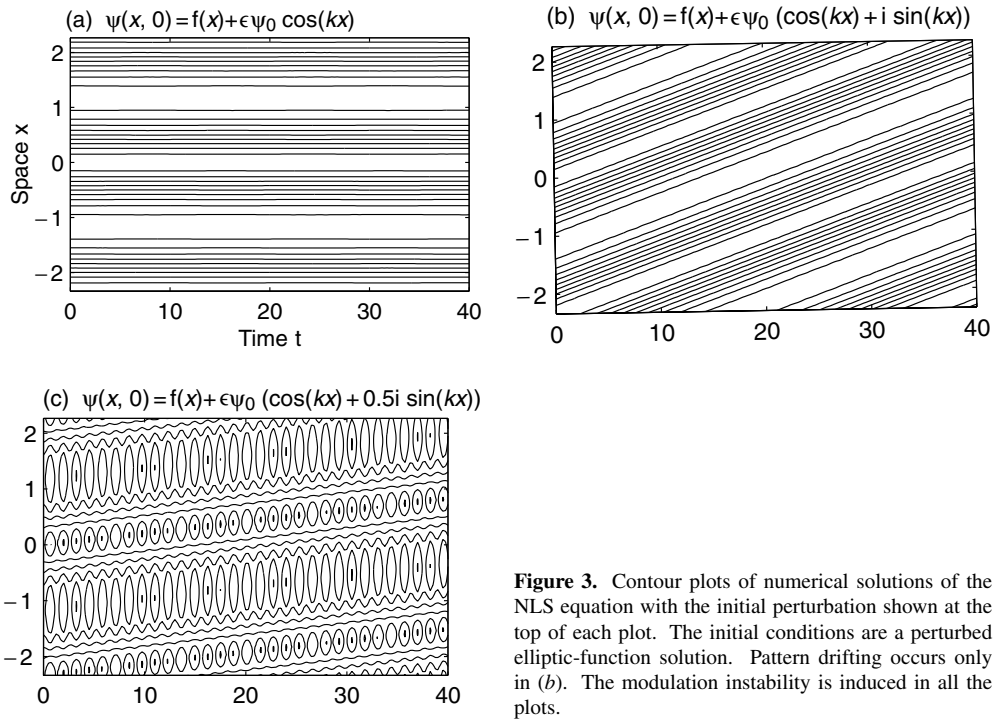

Figure 3. Contour plots of numerical solutions of the NLS equation with the initial perturbation shown at the top of each plot. The initial conditions are a perturbed elliptic-function solution. Pattern drifting occurs only in (*b*). The modulation instability is induced in all the plots.

Let the elliptic-function solution (11) be perturbed so that the initial condition reads

$$\psi(x,0) = f(x) + \epsilon\psi_0[Y_1\cos(kx) + Y_2\sin(kx)] \tag{12}$$

where all quantities are as defined previously. Choosing different values of Y_1 and Y_2, we numerically integrate the NLS equation under the periodic boundary condition and find that the pattern drifts when the elliptic-function solution is disturbed by a circularly-polarized initial perturbation (i.e., $|Y_1| \neq 0$, $|Y_2| \neq 0$ and Y_2/Y_1 is complex in equation (12)), but does not when disturbed by a linearly polarized perturbation. This is the same as for the perturbed spatially homogeneous solution. Figure 3 shows the results of the simulation for $N = \psi_0^2 = 4$, $\epsilon = 0.01$ and $k = 0.9k_0$, where $k_0 = \sqrt{2N}$ is the critical value of the wavenumber for modulation instability. In figure 3(*a*), the initial condition contains only a cosine term and there is no drifting. In figure 3(*b*), the initial perturbation is circularly polarized, and the drifting is induced but the modulation instability is not. Therefore pattern drifting is not necessarily related to modulation instability. The drifting velocity for the perturbed elliptic-function solution is constant. In figure 3(*c*), both the modulation instability and the pattern drifting are induced by circularly-polarized initial perturbation.

The perturbation analysis given in section 3 was performed near the spatially homogeneous solution. The results of the analysis, however, is also applicable to the elliptic-function solution, as shown in figure 4. The solid curve in the figure is for the amplitude square of the exact solution, $[f(x)]^2$, where $f(x)$ is given in equation (11). The dotted curve is given by the perturbation analysis, i.e., given by equation (4) with $\phi(t) = 0$ and $r(t) = r^* = 2\sqrt{k_0^3|\delta k|}$. (At $r(t) = r^*$, the potential in equation (5) reaches its minimum.) The two curves agree with each other very well. Therefore the elliptic-function solution can be approximately given by the perturbation-analytical wavefunction (4) with $\phi(t) = 0$ and $r = r^*$ (i.e., when the potential in equation (5) reaches its minimum). In this sense, the elliptic-function solution corresponds

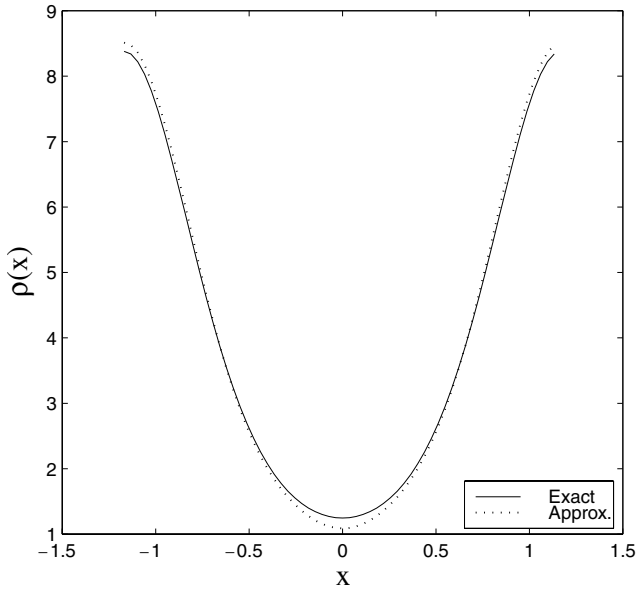

Figure 4. Applicability of the perturbation analysis given in section 3 to the perturbed elliptic-function solution. The figure is for $N = 4$ and $k = 0.95k_0$. The solid curve is for the exact elliptic-function solution (11). The dotted curve is given by the perturbation analysis, i.e., equation (4) with $r = 2\sqrt{k_0^3|\delta k|}$ and $\phi = 0$.

to the minimum of the potential in equation (5) at $r = r^*$.

5. Pattern drifting in the perturbed NLS equation

Finally, we report that pattern drifting is also observed in the one-dimensional perturbed NLS equation

$$\mathrm{i}\partial_t\psi + \partial_x^2\psi + (|\psi|^2 - g|\psi|^4)\psi = 0 \tag{13}$$

where g is a small parameter. The equation has the following spatially homogeneous solution:

$$\tilde{\psi}_h(x,t) = \psi_0\,\mathrm{e}^{\mathrm{i}(|\psi_0|^2 - g|\psi_0|^4)t}. \tag{14}$$

We numerically integrate equation (13) with the periodic boundary and initial conditions (3). The simulation results (not given here) show a drifting phenomenon similar to that for the (unperturbed-cubic) NLS equation shown in figure 1; a linearly polarized initial perturbation does not induce pattern drifting, but a circularly-polarized initial perturbation does.

An interesting numerical observation is that pattern drifting suppresses pattern competition, as shown in figure 5. (The one-dimensional NLS equation has two types of solution patterns: the bright and the dark soliton pattern, see, for example, [7] and references therein. Pattern competition is the phenomena that the two types of solution pattern co-exist and appear randomly: no single pattern dominates over the other and it is impossible to predict what pattern type will emerge in the next moment. The mechanism of pattern competition is the crossing of the homoclinic point [7], whose existence is due to the bi-stability of the nonlinear term in the NLS equation.) In figure 5(*a*), one sees pattern competition but no pattern drifting because we have applied a linearly polarized perturbation given by

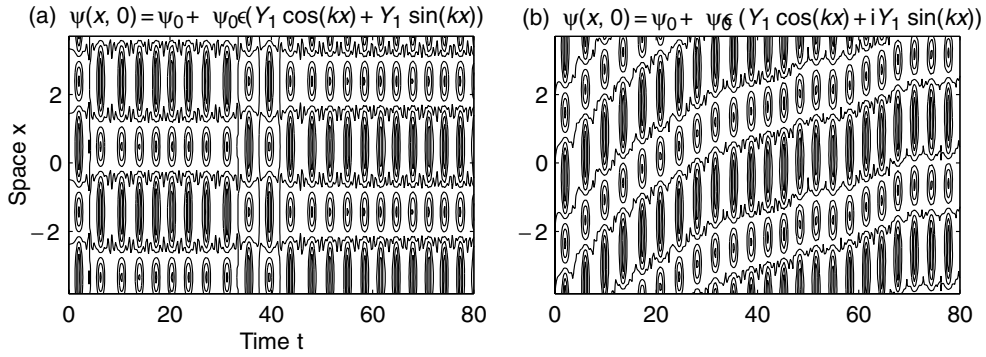

Figure 5. Contour plots of solutions of the perturbed NLS equation (13) with $\psi_0 = 2$, $\epsilon = 0.01$, $g = 0.05$ and $k = 0.75k_0$. (*a*) Under a linearly polarized perturbation, pattern drifting is not induced, but pattern competition is. (*b*) Under a circularly polarized initial perturbation, pattern drifting is also induced, which suppresses the pattern competition observed in (*a*).

$Y_2 = Y_1 = -2\mathrm{i}\sqrt{(k_0/k)^2 - 1}$. In figure 5(*b*), however, both pattern competition and drifting are induced under a circularly-polarized initial perturbation with $Y_2 = \mathrm{e}^{\mathrm{i}\pi/2}Y_1$, where $Y_1 = -2\mathrm{i}\sqrt{(k_0/k)^2 - 1}$. One can see from figure 5(*b*) that the 'solitons' line up, i.e., the pattern is regularized by the pattern drifting. Therefore, pattern drifting may be used to control irregularity or spatial-temporal chaos caused by pattern competition.

6. Conclusions

The drifting of the solution pattern is a common phenomenon in the NLS equation (1). It occurs when the spatially homogeneous solution (2) or the elliptic-function solution (11) is disturbed by a perturbation proportional to $(Y_1 \cos kx + Y_2 \sin kx)$, where Y_1 and Y_2 are nonzero complex numbers and are not along the same line in the complex plane. Pattern drifting also occurs when the spatially homogeneous solution (14) of the perturbed NLS equation (13) is disturbed by a harmonic perturbation. The pattern drifting breaks the reflectional symmetry of the solutions. It is possible to induce pattern drifting without modulation instability. It is expected that pattern drifting and the consequent symmetry breaking occur also in the one-dimensional attractive NLS equation, in a multi-dimensional NLS equation and in other evolution equations.

Perturbation analysis provides an approximate solution (4) to the one-dimensional cubic-repulsive NLS equation and expression (7) for the drifting velocity, which agree well with the results obtained from direct numerical simulations. Drifting velocity is proportional to the angular velocity of a rotation in the space spanned by the order functions introduced in the perturbation analysis. It is expected that the perturbation method can also be applied to study other evolution equations.

Acknowledgments

This work was partially supported by the Research Grant Committee of Hong Kong grants nos DAG99/00.SC23 and HKUST606/95P.

Appendix

In this appendix we derive equation (4) using perturbation analysis.

At first we change the form of the NLS equation (1) by applying the following three transformations. (i) We apply a (trivial) gauge transformation so that the spatially homogeneous solution of the NLS equation is a constant, i.e., $\psi_h(x,t) = \psi_0 = \sqrt{N}$, where $N = \frac{1}{L}\int_{-L/2}^{L/2} |\psi(x,t)|^2\,\mathrm{d}x$ is the total number of quasi-particles. Under the transformation, the NLS equation becomes

$$\mathrm{i}\partial_t\psi(x,t) + \partial_x^2\psi(x,t) + (|\psi(x,t)|^2 - N)\psi(x,t) = 0. \tag{15}$$

(ii) We write a solution of equation (15) as, as in the main text, $\psi(x,t) = \sqrt{\rho(x,t)}\exp[\mathrm{i}\theta(x,t)]$, where $\rho(x,t)$ is the non-negative square-root amplitude function and $\theta(x,t)$ is the real-valued phase function of the solution. (iii) We use the scaled space variable $x' = kx$, where k is the fundamental wavenumber, and the scaled time variable $t' = \omega t$, where ω is the fundamental frequency. Using the scaled variables (and omitting the prime in the scaled variables x' and t' for simplicity), the square-root amplitude function and the phase function satisfy the following equations:

$$\begin{aligned} &\frac{k^2}{2\rho}\partial_x^2\rho - \frac{k^2}{4\rho^2}(\partial_x\rho)^2 - \omega\partial_t\theta - k^2(\partial_x\theta)^2 + (\rho - N) = 0 \\ &k^2\rho\partial_x^2\theta + k^2(\partial_x\rho)(\partial_x\theta) + \frac{\omega}{2}\partial_t\rho = 0 \qquad -\frac{L}{2} \leqslant x \leqslant \frac{L}{2} \qquad t \geqslant 0. \end{aligned} \tag{16}$$

We study this equation under the periodic boundary condition and the conservation of the quasi-particle number.

We are interested in a solution to equation (16), which is near the steady-state solution, i.e., $\rho \approx \rho_0 = N$ and $\theta \approx \theta_0 = 0$. Let such a solution be written as

$$\begin{aligned} \rho &= \rho_0 + \bar{\epsilon}\rho_1 + \bar{\epsilon}^2\rho_2 + \bar{\epsilon}^3\rho_3 + \cdots \\ \theta &= \theta_0 + \bar{\epsilon}\theta_1 + \bar{\epsilon}^2\theta_2 + \bar{\epsilon}^3\theta_3 + \cdots \end{aligned} \tag{17}$$

where $\bar{\epsilon}$ is the perturbation parameter, and the subscripts of the variables ρ and θ indicate the order of approximation. Furthermore, we are interested only in the case where the wavenumber k in equation (16) is close to its critical value for modulation instability (i.e., $k \approx k_0 = \sqrt{2N}$) and that the frequency ω is close to zero. Therefore we write

$$\begin{aligned} k &= k_0 + \bar{\epsilon}k_1 + \bar{\epsilon}^2k_2 + \bar{\epsilon}^3k_3 + \cdots \\ \omega &= \omega_0 + \bar{\epsilon} + \bar{\epsilon}^2\omega_2 + \bar{\epsilon}^3\omega_3 + \cdots \end{aligned} \tag{18}$$

where the subscripts of the variables k and ω indicate the order of approximation.

Substituting equations (17) and (18) into (16), we have a sequence of equations for $\rho_i(x,t)$ and $\theta_i(x,t)$, $i = 0, 1, 2, \ldots$, for different orders in $\bar{\epsilon}$. For the zeroth order in $\bar{\epsilon}$, we have the steady-state solution

$$\rho_0(x,t) = N \qquad \theta_0(x,t) = 0. \tag{19}$$

For the first order in $\bar{\epsilon}$, we have $\partial_x^2\rho_1 + \frac{2\rho_0}{k_0^2}\rho_1 = 0$ and $\partial_x^2\theta_1 = 0$. The general solution of these equations is $\rho_1(x,t) = A(t)\exp(\mathrm{i}\frac{\sqrt{2\rho_0}}{k_0}x) + B(t)\exp(-\mathrm{i}\frac{\sqrt{2\rho_0}}{k_0}x)$ and $\theta_1(x,t) = C(t) + D(t)x$, where $A(t)$, $B(t)$, $C(t)$ and $D(t)$ are all functions of time only. In order to satisfy the periodic boundary condition, we must choose $D(t) = 0$ and $\sqrt{2\rho_0}/k_0 = 0, 1, 2, \ldots$. We take $\sqrt{2\rho_0}/k_0 = 1$, i.e., $k_0 = \sqrt{2N}$, because expansion (17) is made for $k \approx k_0$. Therefore

$$\begin{aligned} \rho_1(x,t) &= A(t)\exp(\mathrm{i}x) + B(t)\exp(-\mathrm{i}x) \\ \theta_1(x,t) &= C(t). \end{aligned} \tag{20}$$

For the second order in $\bar{\epsilon}$, we have

$$\begin{aligned}
&\partial_x^2\rho_2 + \rho_2 + \frac{3}{2\rho_0}A(t)^2\exp(\mathrm{i}2x) + \frac{3}{2\rho_0}B(t)^2\exp(-\mathrm{i}2x) - \partial_t C(t) \\
&\qquad + \frac{A(t)B(t)}{\rho_0} - \frac{\sqrt{2\rho_0}k_1}{\rho_0}A(t)\exp(\mathrm{i}x) - \frac{\sqrt{2\rho_0}k_1}{\rho_0}B(t)\exp(-\mathrm{i}x) = 0 \qquad (21)\\
&\partial_x^2\theta_2 + \frac{1}{8\rho_0^2}A(t)\exp(\mathrm{i}x) + \frac{1}{8\rho_0^2}B(t)\exp(-\mathrm{i}x) = 0
\end{aligned}$$

which has the solution

$$\begin{aligned}
\rho_2(x,t) &= \frac{1}{2\rho_0}(A(t)^2\exp(\mathrm{i}2x) + B(t)^2\exp(-\mathrm{i}2x)) + \left[\partial_t C(t) - \frac{A(t)B(t)}{\rho_0}\right] \\
&\quad - \frac{\mathrm{i}k_1}{\sqrt{2\rho_0}}[A(t)x\exp(\mathrm{i}x) - B(t)x\exp(-\mathrm{i}x)] \qquad (22)\\
\theta_2(x,t) &= \frac{1}{4\rho_0^2}[\partial_t A(t)\exp(\mathrm{i}x) + \partial_t B(t)\exp(-\mathrm{i}x)].
\end{aligned}$$

In the expression for ρ_2 above, the term $[\partial_t C(t) - A(t)B(t)/\rho_0]$ should be zero due to the conservation of the quasi-particles. Thus $C(t) = \frac{1}{\rho_0}\int_0^t A(\tau)B(\tau)\,\mathrm{d}\tau$. Furthermore, the last term in the expression for ρ_2 in equation (22), $-(\mathrm{i}k_1/\sqrt{2\rho_0})[A(t)x\exp(\mathrm{i}x) - B(t)x\exp(-\mathrm{i}x)]$, should also be zero because of the periodic boundary condition, i.e., $k_1 = 0$. Hence

$$\begin{aligned}
\rho_2(x,t) &= \frac{1}{2\rho_0}[A(t)^2\exp(\mathrm{i}2x) + B(t)^2\exp(-\mathrm{i}2x)] \\
\theta_2(x,t) &= \frac{1}{4\rho_0^2}[\partial_t A(t)\exp(\mathrm{i}x) + \partial_t B(t)\exp(-\mathrm{i}x)].
\end{aligned} \qquad (23)$$

j For the third order in $\bar{\epsilon}$, the equations for $\rho_3(x,t)$ and $\theta_3(x,t)$ are

$$\begin{aligned}
&\partial_x^2\rho_3 + \rho_3 + \frac{3}{2\rho_0}[(A(t))^3\exp(\mathrm{i}3x) + (B(t))^3\exp(\mathrm{i}3x)] - \frac{A(t)B(t)\omega_2}{\rho_0} \\
&\qquad - \frac{\exp(\mathrm{i}x)}{4\rho_0^2}[\partial_t^2 A(t) + 2A(t)^2B(t) + 2(2\rho_0)^{3/2}k_2A(t)] \\
&\qquad - \frac{\exp(-\mathrm{i}x)}{4\rho_0^2}[\partial_t^2 B(t) + 2B(t)^2A(t) + 2(2\rho_0)^{3/2}k_2B(t)] = 0 \qquad (24)\\
&\partial_x^2\theta_3 - \frac{1}{4\rho_0^3}\Bigg[A(t)\partial_t A(t)\exp(\mathrm{i}2x) + B(t)\partial_t B(t)\exp(-\mathrm{i}2x)) \\
&\qquad + \frac{\omega_2}{4\rho_0^2}(\partial_t A(t)\exp(\mathrm{i}x) + \partial_t B(t)\exp(-\mathrm{i}x)\Bigg] = 0.
\end{aligned}$$

Again, we use the periodic boundary condition and the conservation of the quasi-particle number to find that the last three terms in the equation for ρ_3 should be eliminated. In other words, $\omega_2 = 0$ and

$$\begin{aligned}
&\frac{\mathrm{d}^2}{\mathrm{d}t^2}A(t) + 2k_0^3(\delta k)A(t) + 2[A(t)]^2B(t) = 0 \\
&\frac{\mathrm{d}^2}{\mathrm{d}t^2}B(t) + 2k_0^3(\delta k)B(t) + 2[B(t)]^2A(t) = 0
\end{aligned} \qquad (25)$$

where $\delta k = k - k_0$. Therefore, $\rho_3(x,t)$ and $\theta_3(x,t)$ are given by

$$\begin{aligned}
\rho_3(x,t) &= \frac{3}{16\rho_0^2}[A(t)^3\exp(\mathrm{i}3x) + B(t)^3\exp(-\mathrm{i}3x)] \\
\theta_3(x,t) &= -\frac{1}{16\rho_0^3}[A(t)\partial_t A(t)\exp(\mathrm{i}2x) + B(t)\partial_t B(t)\exp(-\mathrm{i}2x)].
\end{aligned} \qquad (26)$$

Adding the solutions $\rho_i(x,t)$, $i = 0, 1, 2, 3$, given in equations (19), (20), (23) and (26), and doing the same for $\theta_i(x,t)$, we have, up to the third order in the perturbation parameter

$$\begin{aligned}\rho(x,t) &= N + [A(t)\exp(\mathrm{i}kx) + B(t)\exp(-\mathrm{i}kx)] \\ &\quad + \frac{1}{2\rho_0}[(A(t))^2\exp(\mathrm{i}2x) + (B(t))^2\exp(-\mathrm{i}2kx)] \\ &\quad - \frac{3}{16\rho_0^2}[(A(t))^3\exp(\mathrm{i}3x) + (B(t))^3\exp(-\mathrm{i}3x)] \\ \theta(x,t) &= \frac{1}{\rho_0}\int_0^t A(\tau)B(\tau)\,\mathrm{d}\tau + \frac{1}{4\rho_0^2}[\partial_t A(t)\exp(\mathrm{i}kx) + \partial_t B(t)\exp(-\mathrm{i}kx)] \\ &\quad - \frac{1}{16\rho_0^3}[A(t)\partial_t A(t)\exp(\mathrm{i}2kx) + B(t)\partial_t B(t)\exp(-\mathrm{i}2kx)].\end{aligned} \tag{27}$$

Here we have come back to the original (un-scaled) space and time variables.

The functions $A(t)$ and $B(t)$ must be complex conjugate to each other so that the square-root amplitude $\rho_1(x,t)$ in equation (20) is real, as it should be. Therefore we write $A(t) = \frac{1}{2}[\alpha(t) - \mathrm{i}\beta(t)]$ and $B(t) = \frac{1}{2}[\alpha(t) + \mathrm{i}\beta(t)]$, where $\alpha(t)$ and $\beta(t)$ are real functions of time and called order functions [7]. From equation (25), the order functions satisfy

$$\begin{aligned}&\frac{\mathrm{d}^2}{\mathrm{d}t^2}\alpha + \frac{1}{2}\alpha\beta^2 + \frac{1}{2}\alpha^3 + 2k_0^3(\delta k)\alpha = 0 \\ &\frac{\mathrm{d}^2}{\mathrm{d}t^2}\beta + \frac{1}{2}\beta\alpha^2 + \frac{1}{2}\beta^3 + 2k_0^3(\delta k)\beta = 0.\end{aligned} \tag{28}$$

These equations define a Hamiltonian system with the Hamiltonian function $H = \frac{1}{2}(\dot{\alpha}^2 + \dot{\beta}^2) + V(\alpha,\beta)$, where $V(\alpha,\beta) = \frac{1}{8}(\alpha^2+\beta^2)^2 + k_0^3(\delta k)(\alpha^2+\beta^2)$ is the potential. In the polar coordinates $(r(t), \phi(t))$ on the $\alpha\beta$-plane, the Hamiltonian is as given in equation (5). Using $r(t)$ and $\phi(t)$, instead of $A(t)$ and $B(t)$, solution (27) of the NLS equation becomes equation (4).

References

[1] Akhmediev N N and Ankiewicz A 1997 *Solitons, Nonlinear Pulses and Beams* (London: Chapman and Hall)
[2] Zakharov V E and Manakov S V 1974 *Theor. Math. Phys.* **19** 551
[3] Ablowitz M J and Herbst B M 1990 *SIAM J. Appl. Math.* **50** 339
[4] Ablowitz M J and Clarkson P A 1991 *Soliton, Nonlinear Evolution Equations and Inverse Scattering* (Cambridge: Cambridge University Press) section 3.3
[5] Yuen H C and Ferguson W E 1978 *Phys. Fluids* **21** 1275
[6] Moon H T 1990 *Phys. Rev. Lett.* **64** 412
[7] Tan Y and Mao J-m 1998 *Phys. Rev.* E **57** 381
[8] Konno K and Wodati M 1975 *Prog. Theor. Phys.* **53** 1652
[9] Sattinger D H and Zurkowski V D 1987 *Physica* D **26** 225
[10] Mao J-m, Liu Z R and Cao Y L 1999 *Phys. Rev.* E **560**
[11] Zak M, Zbilut J P and Meyers R E 1997 *From Instability to Intelligence, Complexity and Predictability in Nonlinear Dynamics* (Berlin: Springer)